PAPER

Check for updates

Bio-inspired nacre-like composites with excellent mechanical properties, gas-barrier function and fire-retardant performances based on self-assembly between hyperbranched poly(amido amine)s and montmorillonite†

Biqiang Jin, [ab] Hao Wang, [a] Hu Xu, [a] Haitao Wu, [a] Wenqiang Wu, [a] Zhaoyang Yuan, [a] Zhendong Huang, [a] Yinghan Wang [ID] *[a] and Jinrong Wu [ID] *[a]

The fabrication of mechanically robust multifunctional nanocomposite (NC) films using simple but effective strategies is a long-term challenge. Inspired by natural nacre, we designed and fabricated high-performance nacre-like NC films (Na-MTM/HBP) through the self-assembly of the hyperbranched poly(amido amine) (HBP) and montmorillonite (Na-MTM) using a vacuum filtration approach. The optimal Na-MTM/HBP NC film shows excellent mechanical strength (106 MPa), which can be attributed to the formation of numerous hydrogen bonds and the electrostatic interactions between hyperbranched HBP and Na-MTM nanosheets. Such films also exhibit excellent gas barrier and fire–fire-retardant owing to the high aspect ratio of the Na-MTM nanosheets. In this work, a class of high-performance NC films exhibiting good mechanical, gas barrier, and flame retardancy properties have been developed. These NC films have great potential in packing or coating materials.

1. Introduction

The development of new generations of materials exhibiting high performance and multiple functionalities for diverse strategic fields, such as building construction, transportation, aerospace, and biotechnology, is constantly in demand.[1–3] Through evolution, nature has found smart ways to create lightweight, strong, and tough structural materials with multiple functionalities, such as nacre, tooth, and bone.[4–6] These structural materials usually exhibit elegant and complex architectures at multiple length scales.[7,8] Thus, mimicking the architecture of natural materials is a clever approach to designing new materials.

The nacreous layer of mollusks comprises alternating layers of brittle inorganic calcium carbonate platelets and biopolymers, and it exhibits remarkably high toughness and resilience.[9–11] The outstanding merits of nacre can be attributed to the hierarchical arrangement of its soft and hard constituents that shape a brick-and-mortar structure.[7,12] The nacre-

inspired design principle is to arrange the hard, reinforcing platelets and energy-dissipating soft polymers into ordered structures.[13,14] Novel methods, including layer-by-layer assembly,[15–17] spray casting,[18] vacuum-filtration-induced self-assembly,[19,20] and magnetic-field-assisted additive manufacturing,[21] have been developed to replicate multifunctional nacres using polymers and inorganic platelets. For instance, Du *et al.*[22] fabricated a nacre-mimetic composite with intrinsic self-healing and shape-programming capabilities by infiltrating a thermally reversible Diels–Alder network polymer into a long-range-ordered lamellar scaffold of alumina platelets. Li *et al.*[9] prepared nacre-like poly (vinyl alcohol)/graphene composite films with superior mechanical, electrical, and biocompatible properties using simple solution casting.

In mimicking a nacre film, the interaction between the soft polymer and hard 2D nanoplatelets is a key factor in the combination of outstanding mechanical properties and functionalities.[23,24] Introducing multiple hydrogen bonds and chemical crosslinks can effectively enhance the interactions between soft polymers and nanoplatelets.[25,26] However, the fabrication of nacre-like materials with superior mechanical properties is usually tedious and time-consuming. Dendric polymers, including hyperbranched polyglycerol and poly(-amido amine), are alternative soft constituents for fabricating strong nacre-like composites because they have various polar groups capable of forming hydrogen bonds and electrostatic interactions with nanoplatelets.[27–30]

[a]State Key Laboratory of Polymer Materials Engineering, College of Polymer Science and Engineering, Sichuan University, Chengdu 610065, China. E-mail: wujinrong@scu.edu.cn; wang_yh@scu.edu.cn

[b]College of Science, Xichang University, Xichang 615000, China

† Electronic supplementary information (ESI) available: Supplemental figures, tables, and pictures; additional experiments and material characterization. See DOI: https://doi.org/10.1039/d2ra07647k
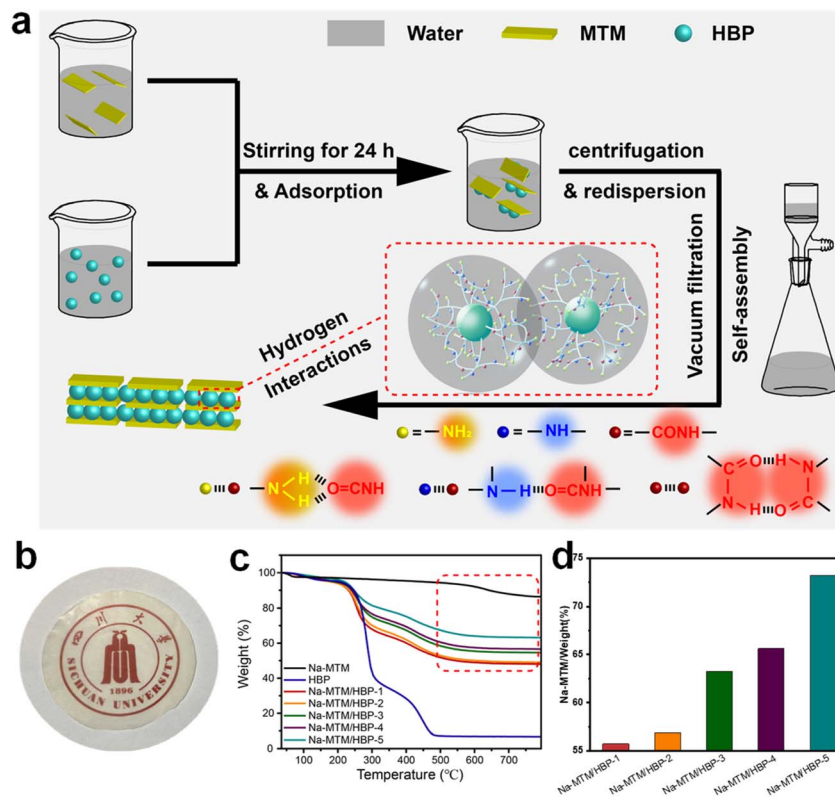
Fig. 1   (a) Schematic diagram for the preparation of Na-MTM/HBP artificial nacre, (b) a photograph of Na-MTM/HBP film, (c) TGA traces for Na-MTM, HBP and Na-MTM/HBPs, (d) Na-MTM weight of Na-MTM/HBPs.

Here, a strong biomimetic artificial nacre with gas barrier and fire-retardant functions was successfully fabricated using vacuum filtration of sodium montmorillonite (Na-MTM) and hyperbranched poly(amido amine) (HBP) (Fig. 1a). Na-MTM and HBP are self-assembled into a biomimetic laminated structure during vacuum filtration with the help of hydrogen bonds and electrostatic interactions. The Na-MTM/HBP nanocomposite (NC) films have mechanical strengths as high as 106 MPa and exhibit excellent gas barrier and flame–fire-retardant. The oxygen permeability (OP) rate is 0.03 mL μm m^{-2} d^{-1} kPa^{-1}. Because of their excellent mechanical, gas barrier, and flame–fire-retardant, these films are promising candidates for diverse applications, including barrier materials for encapsulation and coating.

2.   Experimental sections

2.1   Materials

N,N'-Methylene diacrylamide (MBA, 99+%) was purchased from Admas Reagent Co. Ltd; 1,6-hexamethylene diamine (HAD, 98%) was purchased from TCI Reagent Co. Ltd; methanol was purchased from Titan Technology Co., Ltd; acetone and deionized water were purchased from Chengdu Kelong Chemical Co., Ltd. Na-MTM was purchased from Shanghai Puzhen Biotechnology Co., Ltd. All the reagents were used as received without further purification.

2.2   Synthesis of soft hyperbranched polymer (HBP)

The HBP was synthesized according to a reported method.[30] Briefly, MBA (12.332 g, 0.08 mol) was added into a round bottom flask equipped with a magnetic stirrer containing mixed solvent of 60 mL methanol and 30 mL deionized water at 30 °C and stirred until it was dissolved totally. Then HAD (9.296 g, 0.08 mol) was dissolved in a beaker containing mixed solvent of 20 mL methanol and 10 mL deionized water and fed into the flask directly. The mixture was stirred at 30 °C for 24 h. After that, the solution was poured into a beaker containing 1000 mL acetone to precipitate at room temperature. The crude product was washed 5 times with acetone to obtain a solid and then dried in a vacuum oven at 50 °C for 48 h.

2.3   Preparation of Na-MTM/HBP composite films

In a typical process, 1.25 g Na-MTM was dissolved in a beaker equipped with a magnetic stirrer containing 250 mL deionized water and stirred for one week. The fully dispersed Na-MTM aqueous solution was collected by centrifuged the mixture at 10 000 rpm for 10 min. The HBP was dissolved to prepared various concentrations of aqueous solution, then equal volume of Na-MTM and HBP aqueous solution were mixed and stirred for 2 days. The mixture was centrifuged and the obtained precipitation was washed with deionized water. After that, the precipitation was ultrasonic dispersed in deionized water and then the dispersed solution was vacuum filtrated with cellulose

acetate filter membrane to obtain Na-MTM/HBP composite film. The obtained film was dried at room temperature, subsequently the cellulose acetate filter membrane was dissolved by acetone to obtain the final Na-MTM/HBP composite films. Different weight percentage of Na-MTM/HBP films were prepared, specifically the weight percentage of Na-MTM in Na-MTM/HBP were 10%, 20%, 30%, 40%, 50%, which were named Na-MTM/HBP-1, Na-MTM/HBP-2, Na-MTM/HBP-3, Na-MTM/HBP-4 and Na-MTM/HBP-5, respectively.

2.4   Characterization

FTIR spectra were recorded on Nicolet iS10 (Nicolet, America) in the range of 4000–400 cm^{-1} at room temperature. The FTIR sample of HBP formed after evaporation of methanol on a piece of KBr plate. The ^1H NMR spectra were measured on a Bruker AV III HD spectrometer operating at 400 MHz in deuterated methanol solution with TMS as reference. DSC tests were performed on a PerkinElmer Diamond 3000 with the mass of all samples ranging from 3 mg to 8 mg. Samples were heated from −50 °C to 150 °C at a heating rate of 10 °C min^{-1}. Transmission electron microscope (TEM) images were taken with a TecNaiG2F20S-TWIN transmission electron microscope at an acceleration voltage of 120 kV. The Na-MTM and Na-MTM/HBP dispersed solution were dropped onto an ultrathin carbon-coated copper grid. The grids were dried for the microstructure test. The content and structure of the Na-MTM/HBP were investigated on XSAM800 (kratos) XPS with an Al Kα X-rays radiation. The Na-MTM/HBP was grinded into powder and dried for high resolution narrow scan of the C 1s, N 1s, O 1s and Si 2p. The ratio of the Na-MTM and HBP in Na-MTM/HBP was measured by TGA (Mettler Toledo, Switzerland). Samples ranging from 3 mg to 8 mg were heated from 35 °C to 800 °C at a heating rate of 10 °C min^{-1} under N_2 flow. The Na-MTM/HBP film was scanned in the range of 400–800 nm by UV-vis (UV-3600 Shimadzu, Japan) to obtain the transmission of the film. Layered structure of fractural surface image was recorded on Nova Nano SEM450. SAXS curves were obtained on D8 Discover (Bruker German) equipped with a 2D VANTEC 500 detector and the working current and voltage were 40 mA and 40 kV, respectively, and the wave length of the X-rays was 0.154 nm. The Zeta potential values of Na-MTM, HBP and Na-MTM/HBPs were determined using a Nano Particle Analyzer. The tensile behavior of the Na-MTM/HBPs were measured by an Instron 5967 universal testing machine with the tensile rate of 10 mm min^{-1}. The Oxygen permeability test was performed using a VAC-V1 gas permeability tester (PERME VCA-V1) according to GB/T1038-2000. The fire-retardant test and combustion test of the Na-MTM/HBP film was carried out according to a reported method.[31]

3.   Results and discussion

3.1   Preparation of HBP and Na-MTM/HBP films

For the preparation of Na-MTM/HBP nacre-like films, HBP was first synthesized using a one-pot Michael addition reaction between MBA and HAD with a molar ratio of 1 ($n_{MBA} : n_{HAD} = 1$)

(ESI Fig. S1†). HBP has a molecular weight of 99 253 g mol^{-1} and a polydispersity of 1.46. FTIR and ^1H NMR were used to examine the molecular structure of HBP (ESI Fig. S2†). As shown in the FTIR spectrum of MBA, 3305 cm^{-1} was assigned to the strong stretching vibration peak of the N–H group; 1658 and 1453 cm^{-1} were assigned to the stretching vibration peaks of the C=O (amide I) and N–H (amide II) groups, respectively; and 992 and 967 cm^{-1} were assigned to the bending vibration peaks of the C=C. As seen in the FTIR spectrum of HBP, the stretching vibration peak of –NH– widened; the characteristic peaks of amide I and amide II were observed at 1648 and 1540 cm^{-1}, respectively; and the characteristic peak of C=C disappeared. As seen in the ^1H NMR spectrum of HBP, the typical proton signals of C=C at 6.25 and 5.70 ppm disappeared, and a new signal belonging to the methylene of –CH_2–CH_2–CONH– in HBP appeared at 2–3 ppm. The FTIR and ^1H NMR results confirmed that all vinyl groups were consumed during the Michael addition reaction, and HBP was successfully synthesized. The percentages of primary amine, secondary amine, and tertiary amine units calculated by integrating the characteristic peaks of HBP in the NMR spectra were 20.5%, 59%, and 20.5%, respectively (ESI Fig. S3†).

The fabrication process of the Na-MTM/HBP NC films is shown in Fig. 1a. The Na-MTM suspension and different concentrations of HBP aqueous solutions were used to prepare a series of Na-MTM/HBP dispersions, which were then redispersed using centrifugation. Finally, Na-MTM/HBP NC films were formed using vacuum infiltration. After their self-assembly during vacuum infiltration, the Na-MTM/HBP NC films exhibited certain light transmittance, as indicated by the logo of Sichuan University visible through the Na-MTM/HBP NC films in Fig. 1b. The transmittance spectra of the Na-MTM/HBP NC films showed that the transmission decreased with HBP concentration in the range of 400–800 nm. The transparency of the Na-MTM/HBP NC films was because of the uniform distribution and orderly arrangement of Na-MTM nanosheets. According to the TGA curves shown in Fig. 1c, the residue weights of the Na-MTM/HBP NC films obtained at 800 °C were 48.07%, 49.03%, 54.56%, 56.61%, and 63.17% for Na-MTM/HBP-1, Na-MTM/HBP-2, Na-MTM/HBP-3, Na-MTM/HBP-4, and Na-MTM/HBP-5, respectively. Further, the approximate amounts of clay in the hybrid NC films were 55.73%, 56.84%, 63.25%, 65.63%, and 73.23% for Na-MTM/HBP-1, Na-MTM/HBP-2, Na-MTM/HBP-3, Na-MTM/HBP-4, and Na-MTM/HBP-5, respectively, as shown in Fig. 1d.

3.2   Structure and morphology of the nacre-like composites

The fracture surfaces of the Na-MTM/HBP NC films are examined using SEM. Fig. 2a and b show that the Na-MTM/HBP building blocks were stacked together, forming a compact lamellar microstructure. Similar to the special "brick-and-mortar" structure of natural nacre, the Na-MTM nanoplatelets acted as bricks and HBP as mortar.

Prominent interlayer gaps were observed between lamellae. SAXS was conducted to quantify the structural periodicities of the pure Na-MTM nanosheets and Na-MTM/HBP NC films to
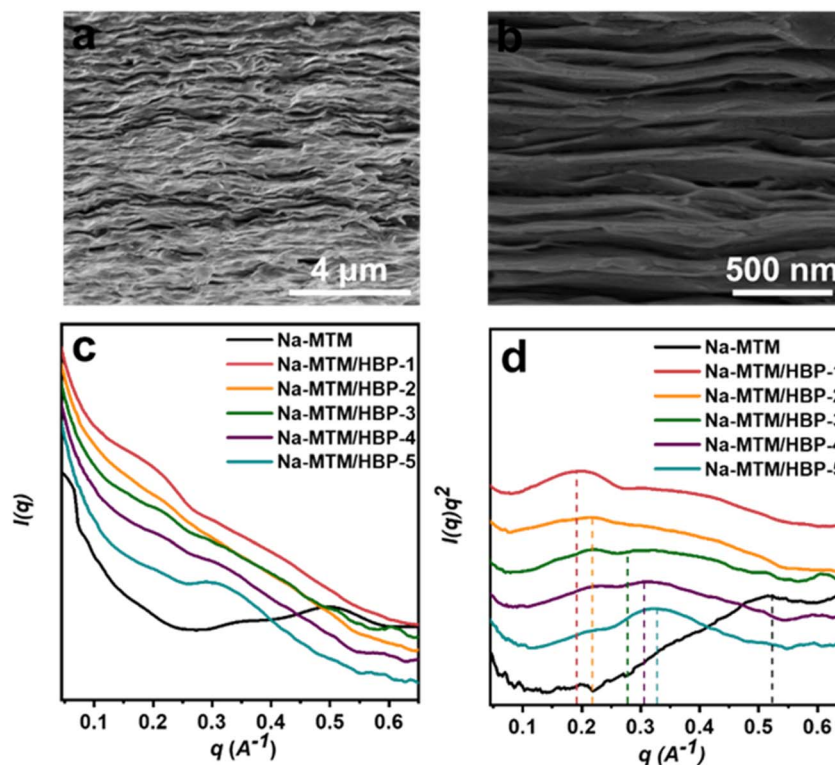
Fig. 2 SEM images of Na-MTM/HBP nacre-mimetic cross section, the scale bars indicate 4 μm (a) and 500 nm (b), 1D SAXS curves of the Na-MTM and Na-MTM/HBP (c), and their Lorentz corrected SAXS plots (d).

investigate the effect of HBP concentration on the interlayer gaps of Na-MTM/HBP NC films, as shown in Fig. 2c and d. The pure Na-MTM layers had a high q value, which gradually decreased with increasing HBP concentration. Therefore, the spacing between the Na-MTM layers of the Na-MTM/HBP NC films was larger than that of the pure Na-MTM nanosheets. As calculated using Bragg's formula,[32] the specific spacings of the Na-MTM layers of Na-MTM/HBP-1, Na-MTM/HBP-2, Na-MTM/HBP-3, Na-MTM/HBP-4, and Na-MTM/HBP-5 NC films were 3.15, 2.90, 2.43, 2.05, and 1.95 nm, respectively. The polymer layer thickness can be calculated to be 1.95, 1.70, 1.23, 0.85, and 0.75 nm by deducting the thicknesses of the clay nanosheets (1.2 nm) from the interlayer distances. These results indicated that each Na-MTM/HBP NC film exhibited periodic structure and that HBP was absorbed into the Na-MTM nanosheet layers.

3.3 Self-assembly mechanism of the nacre-like composites

In mimicking a nacre with superior mechanical properties and multiple functionalities, the interactions between the soft polymer and the hard 2D nanoplatelets play a key role. The hypothetical mechanism for the fabricated Na-MTM/HBP NC film is shown in Fig. 1a. The self-assembly of the NC film was mainly accomplished by the hydrogen and electrostatic interactions between the amino groups in HBP and Na-MTMs, making the structure stable. The TEM images of the Na-MTM nanosheets before and after absorbing the HBP molecules are shown in Fig. 3a and b. The pure Na-MTM nanosheets easily aggregated, but the aggregation of Na-MTM weakened after the

integration of HBP molecules. This phenomenon was attributed to the strong interactions between HBP and Na-MTMs that may result in the adsorption of HBP into Na-MTM nanoplatelet laminates.

The interfacial interactions were further investigated by analyzing the chemical structure of the Na-MTM/HBP NC films using XPS and FTIR. As shown in the XPS wide spectrum of Na-MTM/HBP NC films in Fig. 3c, the relative content of Si increased with the amount of Na-MTM. This result was attributed to the Si component of Na-MTM. Three characteristic peaks were observed in the C 1s core-level spectrum of Na-MTM/HBP (ESI Fig. S4a†) and assigned to C–C/C–H (284.8 eV), C–N (285.8 eV), and C=O (287.8 eV) for HBP. In addition, the relative contents of primary amine (401.5 eV), secondary amine (399.6 eV), and tertiary amine (398.9 eV) were determined from the N 1s core-level spectrum of Na-MTM/HBP (ESI Fig. S4b†) and calculated to be 19.3%, 61.4%, and 19.3%, respectively. These values were consistent with the NMR results. The large number of amino groups in HBP caused the formation of hydrogen bonds between HBP and Na-MTM. As shown in the C 1s core-level spectrum of Na-MTM/HBP (ESI Fig. S4c†), (HBP) C=O (531.3 eV) and (Na-MTM) O (532.0 eV) appeared simultaneously. This finding illustrated that HBP molecules were absorbed by Na-MTM. FTIR measurements were also used to investigate the absorption of HBP in Na-MTM. Fig. 3d shows that the FTIR spectrum of pure Na-MTM displayed stretching bands at 1039 cm⁻¹ for Si–O–Si stretching and 1639 cm⁻¹ for –OH bending. In addition, the FTIR spectrum of HBP exhibited two
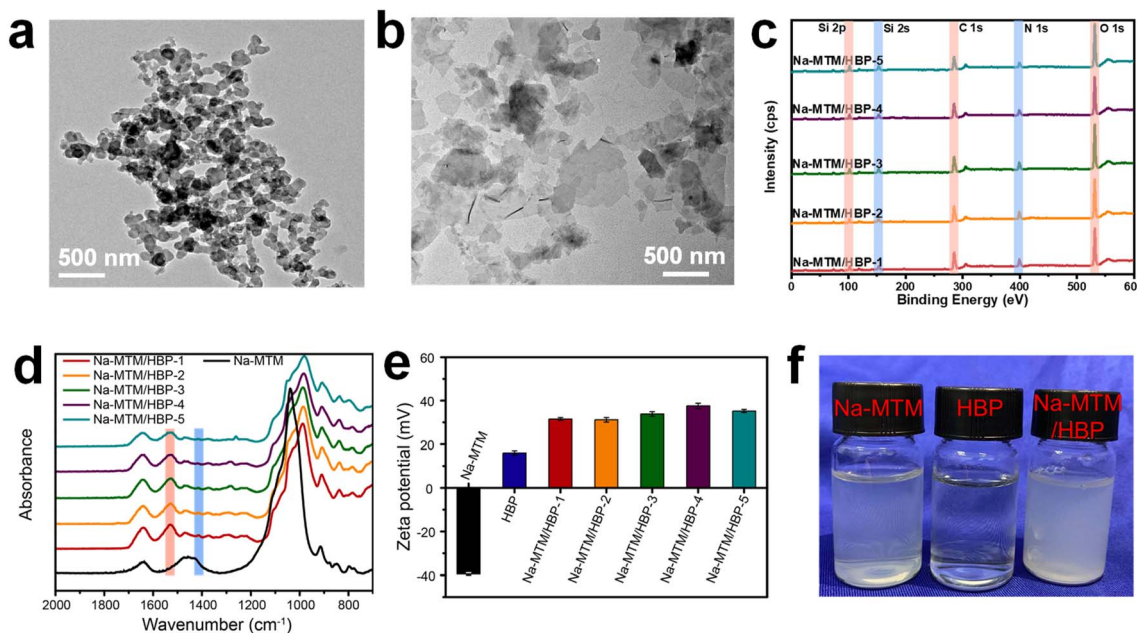
Fig. 3 (a and b) TEM images of MTM nanosheets before and after adsorbing HBP molecules, (c) XPS wide spectrum of Na-MTM/HBPs, (d) FT-IR spectra of Na-MTM and Na-MTM/HBP nanosheets, (e) zeta potentials of Na-MTM, HBP and Na-MTM/HBPs, (f) photographs of Na-MTM suspension liquid, HBP solutions and Na-MTM/HBP suspension liquid.

characteristic peaks: the bending vibration peak of –NH– at 1556 cm^{-1} and the stretching vibration peak of C–N at 1414 cm^{-1}. For the Na-MTM/HBP NC films, the FTIR signals combined the characteristic peaks of HBP and Na-MTM. A comparison of peak positions in HBP and Na-MTM/HBP revealed that the absorption peaks of the amide I band and the amide II band shifted in Na-MTM/HBP NC films (ESI Fig. S5†). This finding further verified that HBP molecules were attached to Na-MTM nanosheets through hydrogen bond interactions.

HBP aqueous solutions and Na-MTM and Na-MTM/HBP suspensions were investigated using a zeta potential instrument to disclose the absorption mechanism between HBP and Na-MTM. Fig. 3e shows that Na-MTM exhibited a strong negative zeta potential ($\zeta = -39.4$ mV). The overall negative charge was due to ionic substitutions in the nanoclay structure, leading to charged basal planes and concomitant Na$^+$ counterion release during delamination in water. The presence of a large number of amino groups on the surface of HBP resulted in positive zeta potential ($\zeta = 16.0$ mV). Upon mixing Na-MTM with HBP, the zeta potential of the Na-MTM/HBP suspension reversed to strongly positive owing to the formation of polyelectrolyte NC films (Na-MTM/HBP). Hence, the entropy driving force of the adsorption of HBP onto Na-MTM was generated by the hydrogen bonding and the release of ordered water molecules at the surface of nano-Na-MTM. Positively charged HBP can integrate strongly with Na-MTM after the release of Na$^+$ counter ions. As shown in Fig. 3f, the Na-MTM/HBP suspension darkened in color when the negatively charged Na-MTM absorbed HBP. This finding further indicated that the integration of Na-MTM and HBP was driven by hydrogen bond

interaction and electrostatic interaction.[33] The NA-MTM/HBP dispersion is self-assembled into a film with a nacre-like structure using vacuum filtration.

3.4 Mechanical properties of Na-MTM/HBP nacre films

Tensile tests were conducted to investigate the influence of HBP on the mechanical properties of nacre-like Na-MTM/HBP NC films. The typical stress–strain curves of HBP and nacre-mimetic NC films are shown in Fig. 4. The tensile strength and fracture strain of HBP were only 16 MPa. The tensile strength improved gradually with the increase in Na-MTM
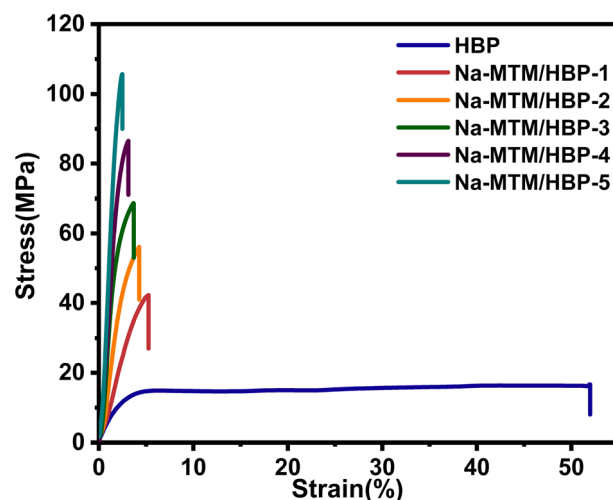

Fig. 4 Typical tensile stress–strain curves of Na-MTM/HBP nacre-like composites.

content. When the Na-MTM content was up to 50%, the tensile strength reached 106 MPa, which is equivalent to that of reported nacre-like Na-MTM-based NC films.[15,34–36] When a high content of inorganic fillers is incorporated into a composite without a periodic structure, the mechanical properties of the materials are usually damaged. In this work, this dilemma was overcome by using vacuum infiltration to create ordered nacre-like structures. Upon the addition of Na-MTM nanoplatelets, the tensile strength was improved owing to the formation of hydrogen bonds and electrostatic interactions between Na-MTM and HBP "brick-and-mortar" structures.

As the Na-MTM content increases from Na-MTM/HBP-1 to Na-MTM/HBP-5, the fracture toughness first increases and then decreases, with a maximum value of 1.61 MJ m^{-3} at Na-MTM/HBP-3. This trend is closely related to Na-MTM content and Na-MTM arrangement regularity in the samples. Because HBP acts as an energy-dissipating soft constituent, it has the highest fracture toughness at 7.69 MJ m^{-3}. We also proposed a fracture model of the robust Na-MTM/HBP NC films. In the first stage, when mechanical stress was applied to the NC film, the slippage and displacement of layers were resisted by the Na-MTM nanosheets. In the next stage, with the increment of stress, the hydrogen bonds and electrostatic interactions began to break, and the Na-MTM nanosheets started to slide over each other, followed by the initiation of cracks that resulted in energy dissipation. Meanwhile, the HBP molecules stretched from the

surface of Na-MTM. When the load continued to increase, the nanosheets were pulled out of the lamella, and fractures occurred. Compared with the complex techniques usually used for Na-MTM nacre-like composites,[25,26] such as the introduction of chemical crosslinking, our method is more easily able to obtain such high-strength nacre-like NC films. Hyperbranched HBP can form numerous hydrogen bonds and electrostatic interactions with Na-MTM nanosheets, resulting in superior mechanical properties. Researchers introduce strong interaction groups with Na-MTM nanosheets *via* complex monomer design and synthesis steps or cross-link the nacre films using a complex curing process to achieve nacre with high strength.

3.5 Multifunction properties of Na-MTM/HBP films

The use of 2D nanosheets usually endows the composites with multiple functionalities, such as electrical, gas barrier, and flame fire-retardant. For the Na-MTM/HBP films, Na-MTM nanoplatelets with a high aspect ratio should be promising owing to their gas barrier and flame fire-retardant. The OP of the Na-MTM/HBP NC films decreased with the addition of Na-MTM nanosheets. In particular, the OP decreased to 0.15, 0.11, 0.09, 0.06, and 0.03 mL μm m^{-2} d^{-1} kPa^{-1} with the introduction of 10%, 20%, 30%, 40%, and 50% Na-MTM nanosheets, respectively. The OP of Na-MTM/HBP NC film with 50% Na-MTM was close to that of commercial ethylene vinyl alcohol film (0.01 mL μm m^{-2} d^{-1} kPa^{-1}).[37] The superior
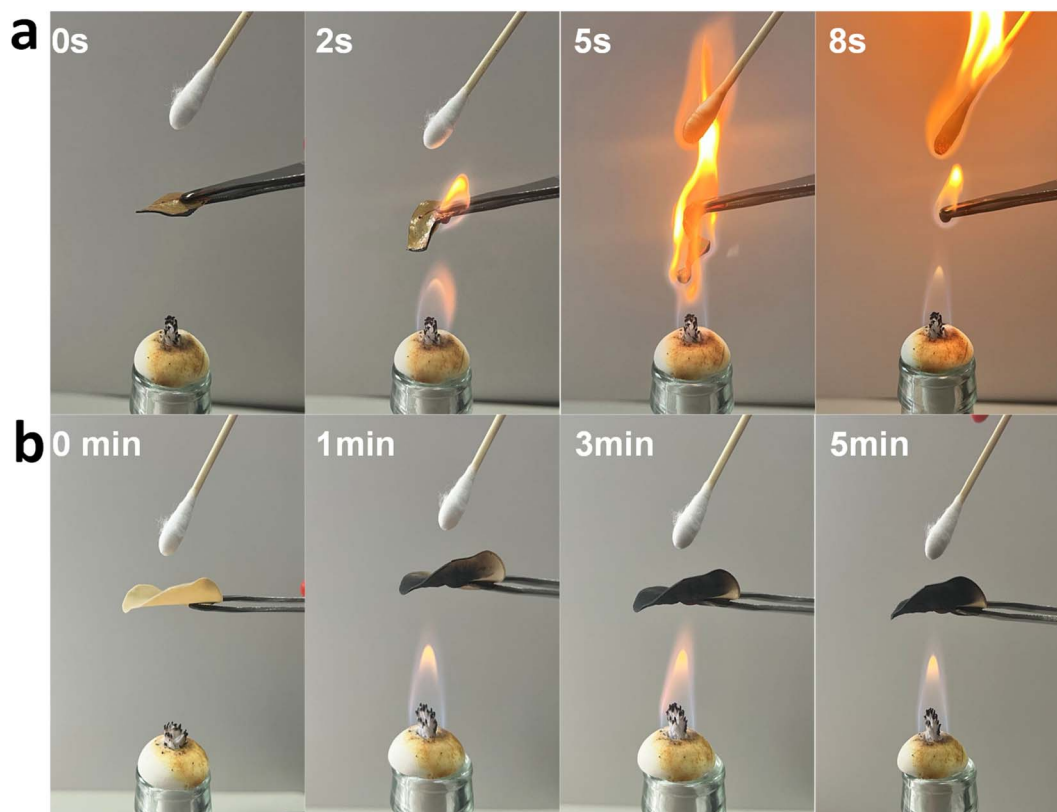

Fig. 5 Fire-retardant test of the pure HBP film (a) and the composite film with 50% Na–MTM content (b) in which the film acts as a fire shield to protect a cotton swab.

gas barrier properties of the Na-MTM/HBP NC films were closely related to the high aspect ratio and orderly arrangement of Na-MTM nanosheets in the NC films.

We then investigated the flame fire-retardant of the Na-MTM/HBP NC films by placing a cotton swab behind the samples in an alcohol flame that had a temperature of 600–800 °C, as shown in Fig. 5. The cotton swab did not catch flame even after 5 min of exposure to the Na-MTM/HBP NC films. Meanwhile, the cotton swab behind pure HBP ignited immediately upon contact with the flame, and the film burned off quickly. The Na-MTM/HBP NC film containing 50% Na-MTM kept its original shape after the sample was placed in the flame for 5 min. However, the sample became charred and turned black because of HBP combustion. The residue material showed good flame resistance. These results suggested that the nacre-like Na-MTM/HBP NC films exhibited superior flame fire-retardant.

4. Conclusions

We successfully prepared nacre-like NC films using vacuum filtration through the self-assembly of HBP molecules with Na-MTM nanosheets. The Na-MTM/HBP NC films exhibited superior mechanical properties owing to the strong interactions between HBP and Na-MTM. The tensile strength of Na-MTM/HBP-5 NC film reached 106 MPa, which is higher than that of many MTM-based composites. The XPS, FTIR, and zeta potential results verified that the self-assembly was driven by hydrogen bonding and electrostatic reactions between Na-MTM and HBP. Moreover, because of the high aspect ratio of Na-MTM, Na-MTM/HBP NC films have good gas barrier and flame fire-retardant. As a result of their excellent mechanical, gas barrier, and flame fire-retardant, these films are promising candidates for use in fire-protection packaging or coating materials.

Conflicts of interest

The authors declare no competing financial interest.

Acknowledgements

References

1 H. Zhao, Z. Yang and L. Guo, *NPG Asia Mater.*, 2018, **10**, 1–22.

2 H. B. Yao, H. Y. Fang, Z. H. Tan, L. H. Wu and S. H. Yu, *Angew. Chem.*, 2010, **122**, 2186–2191.

3 M. E. Launey, E. Munch, D. H. Alsem, H. B. Barth, E. Saiz, A. P. Tomsia and R. O. Ritchie, *Acta Mater.*, 2009, **57**, 2919–2932.

4 F. Libonati and M. J. Buehler, *Adv. Eng. Mater.*, 2017, **19**, 1–19.

5 M. Eder, S. Amini and P. Fratzl, *Science*, 2018, **362**, 543–547.

6 H. Zhao, Z. Yang and L. Guo, *NPG Asia Mater.*, 2018, **10**, 1–22.

7 U. G. K. Wegst, H. Bai, E. Saiz, A. P. Tomsia and R. O. Ritchie, *Nat. Mater.*, 2015, **14**, 23–36.

8 R. L. Truby and J. A. Lewis, *Nature*, 2016, **540**, 371–378.

9 Y. Q. Li, T. Yu, T. Y. Yang, L. X. Zheng and K. Liao, *Adv. Mater.*, 2012, **24**, 3426–3431.

10 Y. Q. Niu, J. H. Liu, C. Aymonier, S. Fermani, D. Kralj, G. Falini and C. H. Zhou, *Chem. Soc. Rev.*, 2022, 7883–7943.

11 X. Li, Z. H. Xu and R. Wang, *Nano Lett.*, 2006, **6**, 2301–2304.

12 J. Wang, Q. Cheng and Z. Tang, *Chem. Soc. Rev.*, 2012, **41**, 1111–1129.

13 P. Ming, Z. Song, S. Gong, Y. Zhang, J. Duan, Q. Zhang, L. Jiang and Q. Cheng, *J. Mater. Chem. A*, 2015, **3**, 21194–21200.

14 S. Xia, Z. Wang, H. Chen, W. Fu, J. Wang, Z. Li and L. Jiang, *ACS Nano*, 2015, **9**, 2167–2172.

15 Z. Tang, N. A. Kotov, S. Magonov and B. Ozturk, *Nat. Mater.*, 2003, **2**, 413–418.

16 L. J. Bonderer, *Science*, 2007, **205411**, 1069–1073.

17 P. Podsiadlo, A. K. Kaushik, E. M. Arruda, A. M. Waas, B. S. Shim, J. Xu, H. Nandivada, B. G. Pumplin, J. Lahann, A. Ramamoorthy and N. A. Kotov, *Science*, 2007, **318**, 80–83.

18 G. Dwivedi, K. Flynn, M. Resnick, S. Sampath and A. Gouldstone, *Adv. Mater.*, 2015, **27**, 3073–3078.

19 J. Wang, Y. Mao, G. Li and H. M. Yin, *Chem. Eng. J.*, 2022, **441**, 136014.

20 X. He, K. Zhang, H. Wang, Y. Zhang, G. Xiao, H. Niu and Y. Yao, *Carbon*, 2022, **199**, 367–378.

21 H. Le Ferrand, F. Bouville, T. P. Niebel and A. R. Studart, *Nat. Mater.*, 2015, **14**, 1172–1179.

22 G. Du, A. Mao, J. Yu, J. Hou, N. Zhao, J. Han, Q. Zhao, W. Gao, T. Xie and H. Bai, *Nat. Commun.*, 2019, **10**, 1–8.

23 Y. Qiang, K. T. Turner and D. Lee, *Nanoscale*, 2021, **13**, 5545–5556.

24 Z. Liu, W. Wang, J. Tan, J. Liu, M. Zhu, B. Zhu and Q. Zhang, *J. Mater. Chem. C*, 2020, **8**, 7170–7180.

25 B. Zhu, N. Jasinski, A. Benitez, M. Noack, D. Park, A. S. Goldmann, C. Barner-Kowollik and A. Walther, *Angew. Chem., Int. Ed.*, 2015, **54**, 8653–8657.

26 W. Hao, L. Zhang, X. Wang, J. Wang, Z. Hu and W. Yang, *RSC Adv.*, 2016, **6**, 1415–1421.

27 W. Hao, S. Ding, L. Zhang, W. Liu and W. Yang, *Chempluschem*, 2014, **79**, 211–216.

28 S. J. Zhang, X. X. Chen, C. H. Cui, L. Ma, Q. Y. Zhong, K. X. Shen, J. Yu, Z. Li, Y. S. Wu, Q. Zhang, Y. L. Cheng, L. He and Y. F. Zhang, *Chin. J. Polym. Sci.*, 2021, **39**, 1319–1327.

29 W. Yang, C. Y. Pan, M. D. Luo and H. Bin Zhang, *Biomacromolecules*, 2010, **11**, 1840–1846.

30 H. Wang, H. Liu, Z. Cao, W. Li, X. Huang, Y. Zhu, F. Ling, H. Xu, Q. Wu, Y. Peng, B. Yang, R. Zhang, O. Kessler, G. Huang and J. Wu, *Proc. Natl. Acad. Sci. U. S. A.*, 2020, **117**, 11299–11305.

31 H. Xie, X. Lai, H. Li, J. Gao, X. Zeng, X. Huang and X. Lin, *Chem. Eng. J.*, 2019, **369**, 8–17.

32 P. S. Singh, P. Ray, Z. Xie and M. Hoang, *J. Membr. Sci.*, 2012, **421–422**, 51–59.

33 W. Zhu, J. Li, J. Lei, Y. Li, T. Chen, T. Duan and W. Yao, *Carbohydr. Polym.*, 2018, **197**, 253–259.

34 H. Yao, Z. Tan, H. Fang and S. Yu, *Angew. Chem., Int. Ed.*, 2010, 10127–10131.

35 F. Lossada, T. Abbasoglu, D. Jiao, D. Hoenders and A. Walther, *Macromol. Rapid Commun.*, 2020, **41**, 2000380.

36 A. Eckert, T. Rudolph, J. Guo, T. Mang and A. Walther, *Adv. Mater.*, 2018, **30**, 1802477–1802484.

37 H. Fukuzumi, T. Saito, S. Iwamoto, Y. Kumamoto, T. Ohdaira, R. Suzuki and A. Isogai, *Biomacromolecules*, 2011, **12**, 4057–4062.